

Rayleigh scattering of photons by helium^{†*}

Chien-ping Lin, Kwok-tsang Cheng, and W. R. Johnson

Department of Physics, University of Notre Dame, Notre Dame, Indiana 46556

(Received 15 January 1975)

We present the results of a Dirac-Hartree-Fock calculation of Rayleigh scattering from He atoms in the energy range 0–500 Ry. The second-order S matrix is used to describe the scattering; the dominant correlation corrections are extracted from the fourth-order S matrix. The scattering amplitude is decomposed into a multipole series and numerical methods are employed to study the multipole amplitudes. For low photon energies the scattering is accurately described by a single electric-dipole amplitude; in this low-energy region correlation corrections modify the second-order amplitude significantly. At higher energies many multipoles contribute to the scattering; above 100 Ry the absorptive part of the second-order amplitude together with the fourth-order correlation corrections are negligibly small. For these very high energies the scattering is accurately described by a scattering form factor.

I. MULTIPOLE EXPANSION OF RAYLEIGH-SCATTERING AMPLITUDE

The present work represents an extension of the theoretical treatment of Rayleigh scattering developed by Brown and co-workers¹ during the 1950's. In these early papers Brown and co-workers treated scattering of hard photons by K electrons in Hg ($Z = 80$). This older treatment employed the Furry bound-interaction representation to evaluate the second-order S matrix and made use of Dirac Coulomb wave functions to describe the electrons.

We start our analysis of the S matrix from a slightly different point. In an attempt to include the electron-electron interaction in the unperturbed Hamiltonian and consequently in the electron wave functions, we employ a Dirac-Hartree-Fock (DHF) description of the atomic electrons. The ground-state DHF potential is introduced in the unperturbed Hamiltonian along with the nuclear Coulomb potential. The use of an unperturbed Hamiltonian including the DHF potential requires the introduction of a DHF counterterm in the interaction Hamiltonian. To second order the expansion of the S matrix is formally identical to that employed by Brown and co-workers; in fourth and higher orders the DHF counterterm gives rise to additional contributions.

In order to gain insight into the effects of electron correlation we carry our calculation to fourth order. We restrict the fourth-order calculation by examining electron-electron interaction terms and DHF counterterms only. We omit electron self-energy and vacuum polarization contributions, which are expected to be small.² Moreover, we limit our treatment of virtual photon exchange to the unretarded Coulomb part (the entire electron-electron interaction in the nonrelativistic limit). We find that the DHF counterterms cancel some of the electron-electron interaction terms in the

fourth-order S matrix. The remaining terms represent fourth-order correlation effects. The present calculation is restricted to two electron atoms for simplicity.

We set up some basic notation in the paragraphs below. In Sec. II we write out the DHF equations and give the expansion of the S matrix to fourth order. Section III is devoted to a theoretical discussion of "perturbed orbitals" and gives the final formulas for the scattering amplitudes. In Secs. IV and V we discuss numerical evaluations of the scattering amplitudes for low-frequency photons (below the photoelectric threshold) and at high frequencies (above threshold), respectively. Our numerical examples are carried out for He ($Z = 2$) where correlation effects are expected to be largest. These studies accomplish the following.

(a) They illustrate the relation of the present scheme to the coupled-Hartree-Fock (CHF) techniques of nonrelativistic quantum mechanics; (b) they reveal sizable correlation corrections at low frequencies; (c) they show the diminishing importance of correlation above threshold; and (d) they indicate the accuracy of a "form-factor" description for energies well above threshold in the case of low- Z atoms.

The differential cross section for Rayleigh scattering can be written³

$$\frac{d\sigma}{d\Omega} = \alpha^2 |M|^2, \quad (1.1)$$

where α is the fine-structure constant and M is the scattering matrix element in units of κ_c . To describe the scattering in the simplest terms we expand M into a multipole series. Let \vec{A} represent the vector potential of a photon with propagation vector \vec{k} and polarization vector $\hat{\epsilon}$. We expand \vec{A} using⁴

$$\vec{A} = \hat{\epsilon} e^{i\vec{k} \cdot \vec{r}} = \sum_{JM\lambda} C_{JM\lambda}(\hat{\epsilon}, \hat{k}) \vec{a}_{JM}^\lambda(\vec{r}), \quad (1.2)$$

where

$$C_{JM\lambda}(\hat{\epsilon}, \hat{k}) = 4\pi i^{J-\lambda} \vec{Y}_{JM}^{(\lambda)}(\hat{k}) \cdot \hat{\epsilon} \quad (1.3)$$

are the multipole expansion coefficients and where the multipole components of the vector potential are

$$\vec{a}_{JM}^0 = j_J(\omega r) \vec{Y}_{JM}(\hat{r}) = j_J(\omega r) \vec{Y}_{JM}^{(0)}(\hat{r}), \quad (1.4a)$$

$$\begin{aligned} \vec{a}_{JM}^1 &= \left(\frac{J+1}{2J+1}\right)^{1/2} j_{J-1}(\omega r) \vec{Y}_{J-1M}(\hat{r}) \\ &\quad - \left(\frac{J}{2J+1}\right)^{1/2} j_{J+1}(\omega r) \vec{Y}_{J+1M}(\hat{r}) \\ &= \frac{1}{\omega} \left(\frac{J+1}{J}\right)^{1/2} \vec{\nabla} \left[\left(j_J(\omega r) - \frac{\omega r j_{J+1}(\omega r)}{J+1} \right) Y_{JM}(\hat{r}) \right] \\ &\quad + \frac{\omega r j_J(\omega r)}{[J(J+1)]^{1/2}} \hat{r} Y_{JM}(\hat{r}). \end{aligned} \quad (1.4b)$$

In Eqs. (1.2)–(1.4) J and M represent the angular momentum of the multipole field and $\lambda = 1$ (0) designates electric (magnetic) multipoles. The photon frequency is denoted by ω , as usual.

Employing the above multipole expansion for both the incident and scattered photon we may extract the dependence of Rayleigh scattering on propagation and polarization directions by writing

$$M = \sum_{JM\lambda; J'M'\lambda'} M_{JM\lambda; J'M'\lambda'} C_{JM\lambda}(\hat{\epsilon}, \hat{k}) C_{J'M'\lambda'}(\hat{\epsilon}', \hat{k}'). \quad (1.5)$$

By virtue of the spherical symmetry of the two-electron ground state the matrix element M is diagonal in the multipole indices,

$$M_{JM\lambda; J'M'\lambda'} = (1/4\pi) \delta_{JJ'} \delta_{MM'} \delta_{\lambda\lambda'} X_{J\lambda}(\omega). \quad (1.6)$$

In Secs. II and III we set up the theoretical background required for a numerical study of the multipole amplitudes $X_{J\lambda}(\omega)$.

II. DHF EQUATIONS AND PERTURBATION EXPANSION

The second-order Rayleigh-scattering matrix element and the dominant correlation corrections are to be evaluated using DHF electron orbitals constructed from the two-electron-ground-state self-consistent potential.⁵ In this section we briefly review the DHF procedure and describe the perturbation expansion of the S matrix based on the DHF orbitals.

Let $Z(r) = Z - Y(r)$ represent the “screened” charge at a distance r from the nucleus. The DHF equations for an electron with principal quantum number n and angular quantum numbers $\kappa = \mp(j + \frac{1}{2})$,

$j = l \pm \frac{1}{2}$, and m is given by

$$[h_0 - \alpha Z(r)/r] u_{n\kappa m}(\vec{r}) = \epsilon_{n\kappa} u_{n\kappa m}(\vec{r}), \quad (2.1)$$

with $h_0 = \vec{\alpha} \cdot \vec{p} + \beta m$. By virtue of the spherical symmetry of $Z(r)$ we can write $u_{n\kappa m}(\vec{r})$ in a spherical basis as

$$u_{n\kappa m}(\vec{r}) = \frac{1}{r} \begin{pmatrix} iG_{n\kappa}(r) & \Omega_{\kappa m}(\hat{r}) \\ F_{n\kappa}(r) & \Omega_{-\kappa m}(\hat{r}) \end{pmatrix}, \quad (2.2)$$

where $G_{n\kappa}(r)$ and $F_{n\kappa}(r)$ are the large- and small-component Dirac radial functions and $\Omega_{\kappa m}(\hat{r})$ is a spherical spinor. From Eqs. (2.1) and (2.2) follow the radial DHF equations

$$\left(\frac{d}{dr} - \frac{\kappa}{r}\right) F_{n\kappa} + \left(m - \epsilon_{n\kappa} - \frac{\alpha Z(r)}{r}\right) G_{n\kappa} = 0, \quad (2.3)$$

$$\left(\frac{d}{dr} + \frac{\kappa}{r}\right) G_{n\kappa} + \left(m + \epsilon_{n\kappa} + \frac{\alpha Z(r)}{r}\right) F_{n\kappa} = 0.$$

For simplicity we designate the two-electron-ground-state radial functions ($n=1$, $\kappa=-1$) by $G_1(r)$ and $F_1(r)$. The corresponding energy eigenvalue is designated by ϵ_1 and the four-component Dirac orbitals are designated by $u_{1m}(r)$ for $m = \pm \frac{1}{2}$. The “screening” charge $Y(r)$ may be written in terms of G_1 and F_1 as

$$Y(r) = \int_0^r dr' (G_1^2 + F_1^2) + r \int_r^\infty \frac{dr'}{r'} (G_1^2 + F_1^2). \quad (2.4)$$

Equations (2.3) and (2.4) are solved self-consistently to give the radial functions $G_1(r)$, $F_1(r)$, and $Y(r)$, along with the eigenvalue ϵ_1 . Having determined $Z(r) = Z - Y(r)$, one may calculate other orbitals of the complete set of solutions to Eq. (2.1) by numerically integrating Eqs. (2.3).

Since we include a screening correction in the electron orbitals we must subtract a screening counterterm from the quantum-electrodynamic interaction Hamiltonian. In the following calculations we adopt the Lorentz-gauge interaction Hamiltonian,

$$\begin{aligned} H_I &= H_1 + H_c, \\ H_1 &= -ie \int d^3r \bar{\psi} \gamma \cdot A \psi, \\ H_c &= -\alpha \int d^3r \bar{\psi} \gamma_4 Y(r) / r \psi. \end{aligned} \quad (2.5)$$

Let us consider the perturbation expansion of the S matrix using Eqs. (2.5) for the interaction Hamiltonian. To second order in e the matrix element M determined from the Feynman diagrams of Fig. 1(a) is

$$\begin{aligned} M_{JM\lambda; J'M'\lambda'}^{(2)} &= \sum_{m=\pm 1/2} \int \int d^3r_1 d^3r_2 [u_{1m}^\dagger(\vec{r}_1) \vec{a}_{J'M'}^\lambda(\vec{r}_1) \cdot \vec{\alpha} S_F(\vec{r}_1, \vec{r}_2, \epsilon_1 + \omega) \vec{\alpha} \cdot \vec{a}_{JM}^\lambda(\vec{r}_2) u_{1m}(\vec{r}_2) \\ &\quad + u_{1m}^\dagger(\vec{r}_1) \vec{\alpha} \cdot \vec{a}_{JM}^\lambda(\vec{r}_1) S_F(\vec{r}_1, \vec{r}_2, \epsilon_1 - \omega) \vec{a}_{J'M'}^\lambda(\vec{r}_2) \cdot \vec{\alpha} u_{1m}(\vec{r}_2)], \end{aligned} \quad (2.6)$$

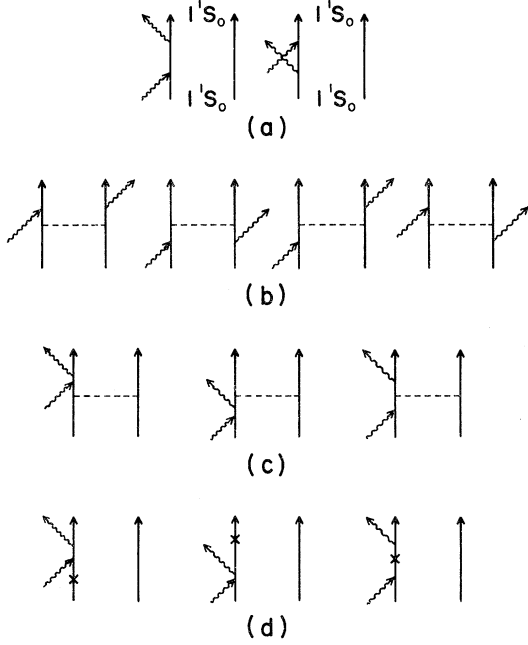


FIG. 1. Solid lines represent bound electrons and wavy lines represent transverse photons, while the dashed lines give the Coulomb interaction. The symbol \times is used to indicate the DHF potential. Diagrams (a) give the second-order terms—coupling of the two electrons to a $1S_0$ state is designated in (a) and understood in the remaining diagrams. Those terms in the fourth-order S matrix considered in the text are illustrated in diagrams (b), (c), and (d). The diagrams (c) are identically canceled by the DHF counter-terms in (d).

where the Feynman propagator $S_F(\vec{x}_1, \vec{x}_2, \epsilon)$ is defined by

$$S_F(\vec{x}_1, \vec{x}_2, \epsilon) = \sum_{\epsilon_n > 0} \frac{u_n(\vec{x}_1)u_n^\dagger(\vec{x}_2)}{\epsilon_n - \epsilon - i\eta} + \sum_{\epsilon_n < 0} \frac{u_n(\vec{x}_1)u_n^\dagger(\vec{x}_2)}{\epsilon_n - \epsilon + i\eta}. \quad (2.7)$$

We will describe the methods used to simplify Eq. (2.6) in Sec. III; before doing so, let us turn our

attention to the higher-order terms in the S matrix.

The effects of electron-electron interaction have been partially accounted for by the DHF screening potential in the one-electron orbitals [and therefore in $S_F(\vec{x}_1, \vec{x}_2, \epsilon)$]. To study the remaining electron-electron effects we look at the next-order terms in the perturbation expansion of the S matrix.

We restrict ourselves to the Feynman diagrams of Figs. 1(b)–1(d), involving one-photon exchange and counterterm corrections to the amplitude. The diagrams of Fig. 1(b) give those corrections for which the absorbed and emitted photons are on different lines, while those of Fig. 1(c) involve both photons interacting with a single electron line. The diagrams of Fig. 1(d) arise from the counterterm H_c in the interaction Hamiltonian.

The electron-electron interaction mediated by a single transverse photon consists of two parts, an instantaneous Coulomb interaction and a retarded Breit interaction. To simplify the algebra with little sacrifice in accuracy we neglect the Breit interaction in comparison with the Coulomb term. Making use of expression (2.4) for $Y(r)$ one finds that the contribution of the diagrams of Fig. 1(c) cancel identically with those of Fig. 1(d). The residual correlation corrections are represented by the Coulomb-interaction diagrams of Fig. 1(b).

In the above discussion we have neglected fourth-order contributions such as electron self-energy and vacuum polarization corrections. We expect these neglected terms to be insignificant compared with the correlation corrections discussed above. Higher-order correlation corrections, which are expected to be important at lower energies, are also neglected—such corrections are contained among the terms of the sixth- and higher-order S matrix.

If we express the matrix element M as a series in α — $M = M^{(2)} + \alpha M^{(4)} + \dots$, where $M^{(2)}$ is given in Eq. (2.6)—we then find from the diagrams of Fig. 1(b) a fourth-order matrix element:

$$M_{JM\lambda; J'M'\lambda'}^{(4)} = - \sum_{\substack{m_1 = \pm 1/2 \\ m_2 = \pm 1/2}} \int \int \int \int \frac{d^3x_1 d^3x_2 d^3x_3 d^3x_4}{|\vec{x}_2 - \vec{x}_3|} \times \{ [u_{1m_1}^\dagger(\vec{x}_1) \vec{a}_{J'M'}^{\lambda'}(\vec{x}_1) \cdot \vec{\alpha} S_F(\vec{x}_1, \vec{x}_2, \epsilon_1 + \omega) u_{1m_1}(\vec{x}_2) + u_{1m_1}^\dagger(\vec{x}_2) S_F(\vec{x}_2, \vec{x}_1, \epsilon_1 - \omega) \vec{a}_{J'M'}^{\lambda'}(\vec{x}_1) \cdot \vec{\alpha} u_{1m_1}(\vec{x}_1)] \\ \times [u_{1m_2}^\dagger(\vec{x}_3) S_F(\vec{x}_3, \vec{x}_4, \epsilon_1 + \omega) \vec{\alpha} \cdot \vec{a}_{JM}^\lambda(\vec{x}_4) u_{1m_2}(\vec{x}_4) + u_{1m_2}^\dagger(\vec{x}_4) \vec{\alpha} \cdot \vec{a}_{JM}^\lambda(\vec{x}_4) S_F(\vec{x}_4, \vec{x}_3, \epsilon_1 - \omega) u_{1m_2}(\vec{x}_3)] \\ - [u_{1m_2}^\dagger(\vec{x}_1) \vec{a}_{J'M'}^{\lambda'}(\vec{x}_1) \cdot \vec{\alpha} S_F(\vec{x}_1, \vec{x}_2, \epsilon_1 + \omega) u_{1m_2}(\vec{x}_2) + u_{1m_2}^\dagger(\vec{x}_2) S_F(\vec{x}_2, \vec{x}_1, \epsilon_1 - \omega) \vec{a}_{J'M'}^{\lambda'}(\vec{x}_1) \cdot \vec{\alpha} u_{1m_2}(\vec{x}_1)] \\ \times [u_{1m_1}^\dagger(\vec{x}_3) S_F(\vec{x}_3, \vec{x}_4, \epsilon_1 + \omega) \vec{\alpha} \cdot \vec{a}_{JM}^\lambda(\vec{x}_4) u_{1m_1}(\vec{x}_4) + u_{1m_1}^\dagger(\vec{x}_4) \vec{\alpha} \cdot \vec{a}_{JM}^\lambda(\vec{x}_4) S_F(\vec{x}_4, \vec{x}_3, \epsilon_1 - \omega) u_{1m_1}(\vec{x}_3)] \}. \quad (2.8)$$

The relative importance of the correlation correction $M^{(4)}$ will be discussed in detail in Secs. IV and V.

III. AUXILIARY FUNCTIONS AND MULTIPOLE AMPLITUDES

To evaluate the expressions for $M^{(2)}$ and $M^{(4)}$ introduced in Sec. II in a convenient way we introduce a family of auxiliary functions $w_{JMm}^\lambda(\omega, \vec{x})$. Following the procedure developed by Brown and co-workers^{1,6} to treat Rayleigh scattering in Hg we set

$$w_{JMm}^\lambda(\omega, \vec{x}) = \int d^3x' S_F(\vec{x}, \vec{x}', \epsilon_1 + \omega) \vec{\alpha} \cdot \vec{a}_{JM}^\lambda(\vec{x}') u_{1m}(\vec{x}'). \quad (3.1)$$

These auxiliary functions satisfy inhomogeneous Dirac equations

$$[h_0 - \alpha Z(x)/x - \epsilon_1 - \omega] w_{JMm}^\lambda(\omega, \vec{x}) = \vec{\alpha} \cdot \vec{a}_{JM}^\lambda u_{1m}(\vec{x}). \quad (3.2)$$

Additional functions $w_{JMm}^\lambda(-\omega, \vec{x})$ with $\omega \rightarrow -\omega$ and $\vec{\alpha} \cdot \vec{a}_{JM}^\lambda \rightarrow \vec{a}_{JM}^\lambda \cdot \vec{\alpha}$ in Eqs. (3.1) and (3.2) are also required. The auxiliary function $w_{JMm}^\lambda(\omega, \vec{x})$ has an obvious physical significance; it is the perturbation of the Dirac orbital $u_{1m}(\vec{x})$ caused by the multipole component $JM\lambda$ of the absorbed photon; $w_{JMm}^\lambda(-\omega, \vec{x})$ is the perturbation caused by the emitted photon. We refer to these auxiliary functions occasionally as perturbed orbitals.

The inhomogeneous differential equations (3.2) may be reduced to a form suitable for numerical evaluation. To simplify the numerical work near $\omega = 0$, we replace the inhomogeneous driving term $\vec{\alpha} \cdot \vec{a}_{JM}^\lambda$ on the right-hand side of Eq. (3.2) for the electric case ($\lambda = 1$) by a mathematically equivalent expression:

$$\vec{\alpha} \cdot \vec{a}_{JM}^\lambda \rightarrow b_{JM} + \vec{\alpha} \cdot \vec{c}_{JM},$$

where

$$b_{JM}(\vec{r}) = i \left(\frac{J+1}{J} \right)^{1/2} \left(j_J(\omega r) - \frac{\omega r j_{J+1}(\omega r)}{J+1} \right) Y_{JM}(\hat{r}), \quad (3.3)$$

$$\vec{c}_{JM}(\vec{r}) = \frac{\omega r j_J(\omega r)}{[J(J+1)]^{1/2}} \hat{r} Y_{JM}(\hat{r}).$$

To show that substitution (3.3) leaves the second- and fourth-order matrix elements unchanged, it is necessary to substitute Eq. (1.4b) into Eqs. (2.6) and (2.8) and to perform partial integrations. The resulting expressions are formally identical to Eqs. (2.6) and (2.8), with $\vec{\alpha} \cdot \vec{a}_{JM}^\lambda$ replaced by the expression given in Eqs. (3.3).

With the above substitution in mind we may expand the functions $w_{JMm}^\lambda(\omega, \vec{r})$ in terms of angu-

lar-momentum states $w_{J\bar{k}\bar{m}}^\lambda(\omega, \vec{r})$. These new auxiliary functions $w_{J\bar{k}\bar{m}}^\lambda(\omega, \vec{r})$ are again solutions to inhomogeneous Dirac equations; they may be expanded in a spherical basis as

$$w_{J\bar{k}\bar{m}}^\lambda(\omega, \vec{r}) = \frac{1}{r} \left(\begin{array}{c} i S_{J\bar{k}}^\lambda(\omega, r) \Omega_{\bar{k}\bar{m}}^\lambda(\hat{r}) \\ T_{J\bar{k}}^\lambda(\omega, r) \Omega_{-\bar{k}\bar{m}}^\lambda(\hat{r}) \end{array} \right). \quad (3.4)$$

The expression for w_{JMm}^λ in terms of $w_{J\bar{k}\bar{m}}^\lambda$ is

$$w_{JMm}^\lambda(\omega, \vec{r}) = \sum_{\bar{k}\bar{m}} c_{\bar{k}\bar{m}}^\lambda w_{J\bar{k}\bar{m}}^\lambda(\omega, \vec{r}), \quad (3.5)$$

where the expansion coefficients $c_{\bar{k}\bar{m}}^\lambda$ are limited by the following selection rules.

(i) For an electric perturbation ($\lambda = 1$) with photon angular momentum J, M , the perturbed orbital quantum numbers $\bar{k}, \bar{j}, \bar{m}$ are given by

$$\bar{k} = -J - 1, \quad \bar{j} = J + \frac{1}{2}, \quad \bar{l} = J, \quad \bar{m} = m + M;$$

$$\bar{k} = J, \quad \bar{j} = J - \frac{1}{2}, \quad \bar{l} = J, \quad \bar{m} = m + M.$$

The corresponding expansion coefficients are

$$c_{\bar{k}\bar{m}}^1 = i (-1)^{J+1/2-\bar{j}} \left(\frac{2(J+1)(2J+1)}{4\pi(2\bar{j}+1)J} \right)^{1/2} \\ \times c(\frac{1}{2} J \bar{j}; \frac{1}{2} 0) c(\frac{1}{2} \bar{j} \bar{j}; m M \bar{m}).$$

(ii) For a magnetic perturbation ($\lambda = 0$) with photon angular momentum J, M , the perturbed orbital quantum numbers $\bar{k}, \bar{j}, \bar{m}$ are

$$\bar{k} = J + 1, \quad \bar{j} = J + \frac{1}{2}, \quad \bar{l} = J + 1, \quad \bar{m} = m + M;$$

$$\bar{k} = -J, \quad \bar{j} = J - \frac{1}{2}, \quad \bar{l} = J - 1, \quad \bar{m} = m + M.$$

The expansion coefficients in this case are

$$c_{\bar{k}\bar{m}}^0 = \frac{i(\bar{k}-1)}{[J(J+1)]^{1/2}} (-1)^{J+1/2-\bar{j}} \left(\frac{2(2J+1)}{4\pi(2\bar{j}+1)} \right)^{1/2} \\ \times c(\frac{1}{2} J \bar{j}; \frac{1}{2} 0) c(\frac{1}{2} \bar{j} \bar{j}; m M \bar{m}). \quad (3.6b)$$

The radial functions $S_{J\bar{k}}^\lambda$ and $T_{J\bar{k}}^\lambda$ of Eq. (3.4) satisfy inhomogeneous radial Dirac equations

$$\left(\frac{d}{dr} - \frac{\bar{k}}{r} \right) T_{J\bar{k}}^\lambda(\pm \omega, r) \\ + \left(m - \epsilon_1 \mp \omega - \frac{\alpha Z(r)}{r} \right) S_{J\bar{k}}^\lambda(\pm \omega, r) = K_{J\bar{k}}^\lambda(\pm \omega, r),$$

$$\left(\frac{d}{dr} + \frac{\bar{k}}{r} \right) S_{J\bar{k}}^\lambda(\pm \omega, r) \\ + \left(m + \epsilon_1 \pm \omega + \frac{\alpha Z(r)}{r} \right) T_{J\bar{k}}^\lambda(\pm \omega, r) = -L_{J\bar{k}}^\lambda(\pm \omega, r), \quad (3.7)$$

with inhomogeneous driving terms given by

$$\left(\begin{array}{c} K_J^0(\pm \omega, r) \\ L_J^0(\pm \omega, r) \end{array} \right) = j_J(\omega r) \left(\begin{array}{c} F_1(r) \\ G_1(r) \end{array} \right), \quad (3.8a)$$

$$\begin{pmatrix} K_J^1(\pm\omega, r) \\ L_J^1(\pm\omega, r) \end{pmatrix} = \left(j_J(\omega r) - \frac{\omega r j_{J+1}(\omega r)}{J+1} \right) \begin{pmatrix} G_1 \\ F_1 \end{pmatrix} \\ \pm \frac{\omega r}{J+1} j_J(\omega r) \begin{pmatrix} F_1 \\ G_1 \end{pmatrix}. \quad (3.8b)$$

Substituting the perturbed orbitals from Eqs. (3.1) and (3.5) back into the expression (2.6) for the second-order matrix element and carrying out the sum over magnetic quantum numbers, we arrive at a remarkably simple expression for the second-order multipole amplitudes:

$$X_{J_1}^{(2)}(\omega) = 2 \frac{J+1}{J} \left(\frac{J+1}{2J+1} [R_J(-J-1, \omega) + R_J(-J-1, -\omega)] + \frac{J}{2J+1} [R_J(J, \omega) + R_J(J, -\omega)] \right), \quad (3.9a)$$

$$X_{J_0}^{(2)}(\omega) = 2 \left(\frac{J+1}{2J+1} [R_J(-J, \omega) + R_J(-J, -\omega)] + \frac{J}{2J+1} [R_J(J+1, \omega) + R_J(J+1, -\omega)] \right), \quad (3.9b)$$

where the radial integrals $R_J(\bar{\kappa}, \pm\omega)$ are given by

$$R_J(\bar{\kappa}, \pm\omega) = \int dr [S_{J\bar{\kappa}}^{\lambda}(\pm\omega, r) K_J^{\lambda}(\pm\omega, r) + T_{J\bar{\kappa}}^{\lambda}(\pm\omega, r) L_J^{\lambda}(\pm\omega, r)] \quad (3.10)$$

for both values of λ : $\lambda=0$ and $\lambda=1$.

Equations (3.7) are solved numerically for various values of ω , and the radial integrals (3.10) are then carried out. The resulting values for the second-order amplitudes are discussed in Secs. IV and V.

We may evaluate the fourth-order correlation

correction given in Eq. (2.8) in terms of the auxiliary functions also. Substituting Eqs. (3.1) and (3.5) into Eq. (2.8) and carrying out the summations over magnetic quantum numbers, we find the following expressions for the fourth-order multipole amplitudes:

$$\begin{aligned} X_{J_1}^{(4)} = & -\frac{2\alpha(J+1)}{J(2J+1)} \operatorname{Re} \left(\frac{2(J+1)}{2J+1} Q_J(-J-1, \omega; -J-1, -\omega) + \frac{2J}{2J+1} Q_J(J, \omega; J, -\omega) \right. \\ & + \frac{J+1}{(2J+1)^2} [Q_J(-J-1, \omega; -J-1, \omega) + Q_J(-J-1, -\omega; -J-1, -\omega)] \\ & - \frac{J}{(2J+1)^2} [Q_J(J, \omega; J, \omega) + Q_J(J, -\omega; J, -\omega)] \\ & \left. + \frac{4J(J+1)}{(2J+1)^2} [Q_J(J, \omega; -J-1, \omega) + Q_J(J, -\omega; -J-1, -\omega)] \right), \quad (3.11a) \end{aligned}$$

$$\begin{aligned} X_{J_0}^{(4)} = & \frac{2\alpha}{2J+1} \operatorname{Re} \left(\frac{J+1}{2J-1} [Q_{J-1}(-J, \omega; -J, \omega) + Q_{J-1}(-J, -\omega; -J, -\omega) + 2Q_{J-1}(-J, \omega; -J, -\omega)] \right. \\ & \left. + \frac{J}{2J+3} [Q_{J+1}(J+1, \omega; J+1, \omega) + Q_{J+1}(J+1, -\omega; J+1, -\omega) + 2Q_{J+1}(J+1, \omega; J+1, -\omega)] \right). \quad (3.11b) \end{aligned}$$

The Slater-type radial integrals Q_L appearing in Eqs. (3.11) are defined by

$$Q_L(\kappa, \omega; \kappa', \omega) = \iint dr_1 dr_2 \frac{r_1^L}{r_1^{L+1}} [S_{J\kappa}^{\lambda}(\omega) G_1 + T_{J\kappa}^{\lambda}(\omega) F_1]_1 [S_{J\kappa'}^{\lambda}(\omega) G_1 + T_{J\kappa'}^{\lambda}(\omega) F_1]_2, \quad (3.12a)$$

$$Q_L(\kappa, \omega; \kappa, -\omega) = \iint dr_1 dr_2 \frac{r_1^L}{r_1^{L+1}} [S_{J\kappa}^{\lambda}(\omega) G_1 + T_{J\kappa}^{\lambda}(\omega) F_1]_1 [S_{J\kappa}^{\lambda}(-\omega) G_1 + T_{J\kappa}^{\lambda}(-\omega) F_1]_2, \quad (3.12b)$$

$$Q_L(\kappa, -\omega; \kappa, \omega) = Q_L^*(\kappa, \omega; \kappa, -\omega), \quad (3.12c)$$

$$Q_L(\kappa, -\omega; \kappa', -\omega) = \iint dr_1 dr_2 \frac{r_1^L}{r_1^{L+1}} [S_{J\kappa}^{\lambda}(-\omega) G_1 + T_{J\kappa}^{\lambda}(-\omega) F_1]_1 [S_{J\kappa'}^{\lambda}(-\omega) G_1 + T_{J\kappa'}^{\lambda}(-\omega) F_1]_2. \quad (3.12d)$$

The entire amplitude to the order considered is given by

$$X_{J\lambda}(\omega) = X_{J\lambda}^{(2)}(\omega) + X_{J\lambda}^{(4)}(\omega).$$

The most difficult numerical step encountered

in evaluating the Rayleigh-scattering amplitude is the numerical solution of the radial differential equations (3.7). Once this step is accomplished one may evaluate the amplitude to second order by computing the radial integrals of Eq. (3.10), and

determine the fourth-order correlation corrections by performing the radial integrals of Eqs. (3.12). In Secs. IV and V we shall discuss the results of our numerical studies in detail.

IV. SCATTERING OF PHOTONS WITH ENERGIES BELOW PHOTOELECTRIC THRESHOLD

Let us consider low-energy photons: photons with energies $\omega < m - \epsilon_1$, the photoemission threshold. In this low-energy region the scattering amplitude is real. The amplitude has poles at photon energies $\omega = \epsilon_1 - \epsilon_n$, the orbital eigenvalue differences. The reality of the amplitude and its singularity structure can be inferred from the behavior of the solutions to the perturbed orbital equations (3.7).

The multipole amplitudes $X_{J\lambda}(\omega)$ are conveniently expressed in terms of frequency-dependent electric and magnetic susceptibilities in the low-frequency region. Let $\alpha_J(\omega)$ represent the electric 2^J -pole susceptibility and $\chi_J(\omega)$ the corresponding magnetic susceptibility. We may write

$$\begin{pmatrix} \alpha_J(\omega) \\ \chi_J(\omega) \end{pmatrix} = \alpha \frac{J(2J+1)!!(2J-1)!!}{(J+1)\omega^{2J}} \begin{pmatrix} X_{J1}(\omega) \\ X_{J0}(\omega) \end{pmatrix} \quad (4.1)$$

$$\begin{aligned} \alpha_1(\omega) = & \frac{2}{3}\alpha \left[\frac{2}{3}[R(-2, \omega) + R(-2, -\omega)] + \frac{1}{3}[R(1, \omega) + R(1, -\omega)] \right. \\ & - \frac{1}{3}\alpha \left\{ \frac{4}{3}Q(-2, \omega; -2, -\omega) + \frac{2}{3}Q(1, \omega; 1, -\omega) + \frac{2}{9}[Q(-2, \omega; -2, \omega) + Q(-2, -\omega; -2, -\omega)] \right. \\ & \left. \left. - \frac{1}{9}[Q(1, \omega; 1, \omega) + Q(1, -\omega; 1, -\omega)] + \frac{8}{9}[Q(1, \omega; -2, \omega) + Q(1, -\omega; -2, -\omega)] \right\} \right], \quad (4.2) \end{aligned}$$

where

$$R(\kappa, \pm\omega) = \int_0^\infty dr r [G_1 S_{1\kappa}(\pm\omega, r) + F_1 T_{1\kappa}(\pm\omega, r)] \quad (4.3)$$

and

$$\begin{aligned} Q(\kappa, \omega; \kappa', \omega') = & \iint dr_1 dr_2 \frac{r_1 r_2}{r_1^2 r_2^2} [G_1 S_{1\kappa}(\omega) + F_1 T_{1\kappa}(\omega)]_1 \\ & \times [G_1 S_{1\kappa'}(\omega') + F_1 T_{1\kappa'}(\omega')]_2. \quad (4.4) \end{aligned}$$

The functions $S_{J\kappa}$ and $T_{J\kappa}$ of course satisfy Eqs. (3.7); however, the driving terms given in Eq. (3.8b) are now replaced by

$$\begin{pmatrix} K_1(r) \\ L_1(r) \end{pmatrix} = r \begin{pmatrix} G_1(r) \\ F_1(r) \end{pmatrix}. \quad (4.5)$$

The procedure employed to calculate the electric polarizability is first to solve Eqs. (3.7) numerically using the driving terms given in Eqs. (4.5) above. The integrals (4.3) and (4.4) are then eval-

uated numerically, and $\alpha_1(\omega)$ is determined from Eq. (4.2).

As an alternative we can consider the Dirac version of the CHF scheme. In the CHF scheme we use the following simpler expression for $\alpha_1(\omega)$:

Since the amplitudes $X_{J\lambda}(\omega)$ grow as ω^{2J} at low frequencies, it follows that the susceptibilities $\alpha_J(\omega)$ and $\chi_J(\omega)$ approach finite limits as $\omega \rightarrow 0$. Corresponding to the decomposition of $X_{J\lambda}(\omega)$ into a second-order DHF part and a fourth-order correlation correction, there is a parallel decomposition of the susceptibilities. The evaluation of susceptibilities to second order by the methods outlined in Sec. III has been considered previously in Ref. 6(a). It has been established in Ref. 6(a) that the second-order calculation of susceptibilities is the generalization to the Dirac theory of the nonrelativistic uncoupled Hartree-Fock (HF) techniques. The fourth-order perturbations give correlation corrections to these HF calculations. Before presenting our numerical results let us digress slightly to discuss the relation between our fourth-order calculation and the coupled Hartree-Fock (CHF) technique for calculating susceptibilities.

As a specific example let us examine the electric polarizability $\alpha_1(\omega)$. If we factor $\frac{1}{3}\omega$ from Eq. (3.8b) and neglect terms of order $(\omega r)^2$ we obtain the following system of equations for $\alpha_1(\omega)$:

$$\begin{aligned} \alpha_1(\omega) = & \frac{2}{3}\alpha \left\{ \frac{2}{3}[\bar{R}(-2, \omega) + \bar{R}(-2, -\omega)] \right. \\ & \left. + \frac{1}{3}[\bar{R}(1, \omega) + \bar{R}(1, -\omega)] \right\}, \quad (4.6) \end{aligned}$$

with

$$\bar{R}(\kappa, \pm\omega) = \int_0^\infty dr r [G_1 \bar{S}_{J\kappa}(\pm\omega, r) + F_1 \bar{T}_{J\kappa}(\pm\omega, r)]. \quad (4.7)$$

Equation (4.6) for $\alpha_1(\omega)$ contains only the second-order terms of Eq. (4.2), and the integrals $\bar{R}(\kappa, \pm\omega)$ in Eq. (4.7) are identical in form to the corresponding second-order expressions of Eq. (4.2). The functions $S_{J\kappa}$ and $T_{J\kappa}$ of Eq. (4.2) are now replaced by more complicated functions $\bar{S}_{J\kappa}$ and $\bar{T}_{J\kappa}$. These modified radial perturbations $\bar{S}_{J\kappa}$ and $\bar{T}_{J\kappa}$ satisfy the inhomogeneous differential equations (3.7); now, however, the driving terms (3.8b) are replaced by the rather involved expressions

$\kappa = 1$:

$$\begin{pmatrix} K_1(r) \\ L_1(r) \end{pmatrix} = \left[r - \alpha \left(-\frac{1}{9} \frac{Y_1(1, \omega; r)}{r} + \frac{4}{9} \frac{Y_1(-2, \omega; r)}{r} + \frac{1}{3} \frac{Y_1(1, -\omega; r)}{r} \right) \right] \begin{pmatrix} G_1(r) \\ F_1(r) \end{pmatrix}, \quad (4.8a)$$

$\kappa = -2$:

$$\begin{pmatrix} K_1(r) \\ L_1(r) \end{pmatrix} = \left[r - \alpha \left(\frac{2}{9} \frac{Y_1(1, \omega; r)}{r} + \frac{1}{9} \frac{Y_1(-2, \omega; r)}{r} + \frac{1}{3} \frac{Y_1(-2, -\omega; r)}{r} \right) \right] \begin{pmatrix} G_1(r) \\ F_1(r) \end{pmatrix}. \quad (4.8b)$$

The functions $Y_1(\kappa, \omega; r)$ of Eqs. (4.8) are given by

$$\begin{aligned} Y_1(\kappa, \pm\omega; r) = & \frac{1}{r} \int_0^r dr r [\bar{S}_{1\kappa}(\pm\omega)G_1 + \bar{T}_{1\kappa}(\pm\omega)F_1] \\ & + r^2 \int_r^\infty dr \frac{1}{r^2} [\bar{S}_{1\kappa}(\pm\omega)G_1 + \bar{T}_{1\kappa}(\pm\omega)F_1]. \end{aligned} \quad (4.9)$$

The inhomogeneous differential equations (3.7) in the CHF scheme become integro-differential equations which can be solved numerically by iterative techniques. A single iteration of Eqs. (3.7) using the driving terms (4.8) with all of the Y_1 functions set to zero gives the second-order results for $\alpha_1(\omega)$ alluded to previously. Continuing the iteration procedure one step further, using the results of the first iteration to evaluate the functions $Y_1(\kappa, \pm\omega, r)$, and then solving Eqs. (3.7) for $\bar{S}_{1\kappa}$, $\bar{T}_{1\kappa}$ yields exactly the results of our fourth-order calculation of Eqs. (4.2). By continuing the iteration of the CHF equations until self-consistent solutions for $\bar{S}_{1\kappa}$ and $\bar{T}_{1\kappa}$ are obtained we arrive at

$\alpha_1(\omega)$, which includes the fourth-order correlation corrections as well as some—but not all—of the sixth- and higher-order corrections.

We can of course write down similar sets of equations for electric and magnetic susceptibilities of higher multipolarity. Moreover, the solutions to the inhomogeneous Dirac equations may be used to determine electric and magnetic shielding factors as well as susceptibilities. To illustrate these remarks we list in Table I values from the second-order, fourth-order, and CHF calculations of several static ($\omega = 0$) susceptibilities and shielding factors, and compare our values with previous nonrelativistic calculations.

In the low-frequency region the Rayleigh-scattering cross section is dominated by the single multipole amplitude $X_{11}(\omega)$ or, equivalently, by the electric polarizability $\alpha_1(\omega)$. We may write

$$\frac{d\sigma}{d\Omega} = \frac{1}{2}(1 + \cos^2\theta)\omega^4[\alpha_1(\omega)]^2 \quad (4.10)$$

as an accurate low-frequency approximation to the differential cross section.

In Fig. 2 we plot theoretical values of $\alpha_1(\omega)$ in the second-, fourth-, and CHF approximations together with semiempirical values for $\alpha_1(\omega)$. The theoretical values of $\alpha_1(\omega)$ given here are in close agreement with previous nonrelativistic calculations.⁷ Our second-order calculation is 5–10% larger than the semiempirical susceptibility,⁸ while our fourth-order values are 5–10% too low. The CHF calculation improves the fourth-order values only slightly. We conclude that the present fourth-order perturbation theory gives the correct order of magnitude of the correlation corrections, but that a precise determination of correlation effects requires a careful evaluation of sixth- and higher-order terms in the S matrix.

TABLE I. Static electric polarizabilities α_1 and α_2 , the magnetic susceptibilities χ_1 and χ_2 , and the electric shielding factors γ_1 and γ_2 are compared with nonrelativistic values. All values are in atomic units. Numbers in parentheses represent powers of 10.

	Second order ^a	Including fourth order	CHF	Nonrelativistic	
				HF	CHF
α_1	1.487	1.294	1.322	1.48 ^b	1.32 ^b
α_2	2.359	2.325	2.326	2.36 ^b	2.33 ^b
χ_1	-2.103 (-5)	-2.103 (-5)	-2.103 (-5)	-2.103 (-5) ^c	
χ_2	6.356 (-5)	7.896 (-5)			
γ_1	1.236		1.000	1.23 ^b	1.00 ^b
γ_2	0.4206		0.3962	0.417 ^b	0.397 ^d

^a The second-order results are consistent with those obtained in Ref. 6(b).

^b A. Dalgarno, Adv. Phys. **11**, 281 (1962).

^c From one-electron integrals computed by E. Clementi, C. C. J. Roothaan, and M. Yoshimine [Phys. Rev. **127**, 1618 (1962)].

^d A. Dalgarno, W. D. Davison, and A. L. Stewart, Proc. R. Soc. Lond. A **257**, 115 (1960).

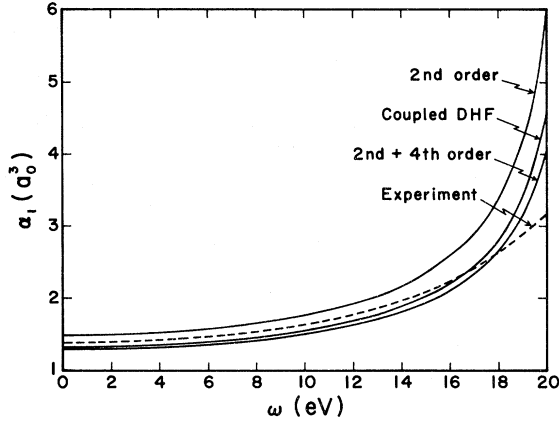


FIG. 2. Present second-order calculation is found to overestimate the low-frequency susceptibility $\alpha_1(\omega)$, while addition of the fourth-order correlation correction gives results which are too small. The CHF results which include some—but not all—of the higher-order correlation effects improve the fourth-order results only slightly. The experimental values are taken from the semiempirical formula of Dalgarno and Kingston (Ref. 8). The disagreement for $\omega > 14$ eV is due partly to the inadequacy of the semiempirical formula at this high frequency.

$$M_X = \frac{1}{2} \sum_{J=1}^{\infty} (2J+1) \left[\left(P_J - \frac{P_J^2}{J(J+1)} \right) X_{J1} + \left(\frac{1}{2}(P_{J-1} + P_{J+1}) + \frac{P_{J-1}^2 + P_{J+1}^2}{2J(J+1)} \right) X_{J0} \right], \quad (5.2a)$$

$$M_Y = \frac{1}{2} \sum_{J=1}^{\infty} (2J+1) \left[\left(P_J - \frac{P_J^2}{J(J+1)} \right) X_{J0} + \left(\frac{1}{2}(P_{J-1} + P_{J+1}) + \frac{P_{J-1}^2 + P_{J+1}^2}{2J(J+1)} \right) X_{J1} \right]. \quad (5.2b)$$

In Eqs. (5.2), $P_J^m(\cos\theta)$ is an associated Legendre function ($P_J = P_J^0$).

The optical theorem relates the imaginary part of the forward-Rayleigh-scattering amplitude to the photoelectric cross section, above the photoelectric threshold. From Eqs. (5.1) and (5.2) we find

$$\sigma_{pe}(\omega) = \frac{2\pi}{\omega} \text{Im}[M_X(\theta=0) + M_Y(\theta=0)] \quad (5.3a)$$

$$= \frac{4\pi}{\omega} \text{Im} \sum_{J=1}^{\infty} (2J+1) [X_{J0}(\omega) + X_{J1}(\omega)]. \quad (5.3b)$$

It is apparent from Eqs. (3.11) that the fourth-order correlation corrections are real, even above threshold; it follows that only the second-order part of $X_{J\lambda}(\omega)$ contributes to the photoelectric cross section in Eqs. (5.3).

In Table II we list values of the second-order multipole amplitudes $X_{J\lambda}^{(2)}(\omega)$ determined by the numerical procedures outlined at the end of Sec. III. We limit the number of multipoles tabulated at each energy to the number needed to obtain am-

V. SCATTERING OF PHOTONS WITH ENERGIES ABOVE PHOTOELECTRIC THRESHOLD

There are two characteristic modifications in the behavior of the multipole amplitudes $X_{J\lambda}(\omega)$ which occur in the high-energy region $\omega > m - \epsilon_1$. First, the solutions to Eqs. (3.7) for the perturbed orbitals become complex; consequently, the multipole amplitudes are complex above threshold. Second, more and more multipoles contribute as energy increases; the description of Rayleigh scattering in terms of the electric polarizability is no longer adequate.

An expression for the Rayleigh scattering of polarized photons in terms of the multipole amplitudes has been derived in Ref. 6(a). If the polarization vectors of the incident and scattered photons ($\hat{\epsilon}, \hat{\epsilon}'$) are decomposed in the two coordinate systems X, Y, Z and X', Y', Z' shown in Fig. 3, then we may write the scattering matrix element M , introduced in Eq. (1.1), as

$$M = \epsilon_X \epsilon'_{X'} M_X + \epsilon_Y \epsilon'_{Y'} M_Y, \quad (5.1)$$

where the amplitudes M_X and M_Y are given in terms of the multipole amplitudes $X_{J\lambda}(\omega)$ by

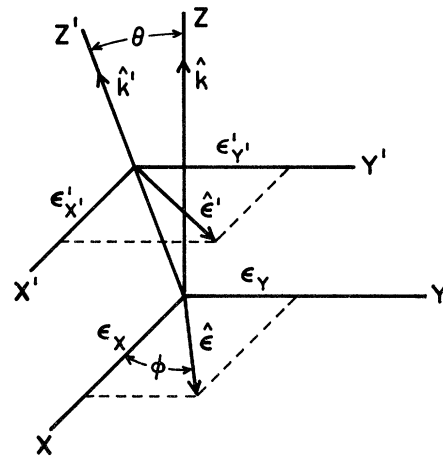


FIG. 3. Axes X, Y, Z are attached to the incident photon ($\hat{k} \parallel Z$), while X', Y', Z' are attached to the scattered photon ($\hat{k}' \parallel Z'$). The outgoing photon is in the XZ plane, while Y' is assumed parallel to Y . The vectors $\hat{\epsilon}$ and $\hat{\epsilon}'$ are the polarization vectors of the incident and scattered photons, respectively.

TABLE II. Second-order multipole amplitudes $X_{J\lambda}^{(2)}(\omega)$ in atomic units tabulated in the format: (Re, Im) (power of 10). Column headings are in the format: (J, λ).

ω (Ry)	(1, 1)	(1, 0)	(2, 1)	(2, 0)	(3, 1)	(3, 0)
5	(-1.096, 0.427) (-2)	(-6.392, 0.0) (-7)	(-4.761, 2.452) (-7)	(-4.249, 0.568) (-11)		
10	(-1.066, 0.138) (-2)	(-2.555, 0.0) (-6)	(-1.785, 0.220) (-6)	(-5.030, 0.073) (-10)		
20	(-1.013, 0.039) (-2)	(-1.019, 0.0) (-5)	(-6.466, 0.151) (-6)	(-7.330, 0.008) (-9)	(-4.286, 0.050) (-9)	(-5.194, 0.004) (-12)
30	(-9.924, 0.173) (-3)	(-2.284, 0.0) (-5)	(-1.408, 0.011) (-5)	(-3.627, 0.001) (-8)	(-2.095, 0.005) (-8)	(-5.758, 0.001) (-11)
40	(-9.804, 0.096) (-3)	(-4.035, 0.0) (-5)	(-2.460, 0.008) (-5)	(-1.130, 0.0) (-7)	(-6.495, 0.006) (-8)	(-3.178, 0.0) (-10)
50	(-9.712, 0.060) (-3)	(-6.256, 0.0) (-5)	(-3.794, 0.007) (-5)	(-2.721, 0.0) (-7)	(-1.561, 0.001) (-7)	(-1.192, 0.0) (-9)
60	(-9.630, 0.041) (-3)	(-8.925, 0.0) (-5)	(-5.395, 0.006) (-5)	(-5.560, 0.0) (-7)	(-3.186, 0.001) (-7)	(-3.492, 0.0) (-9)
70	(-9.548, 0.029) (-3)	(-1.201, 0.0) (-4)	(-7.249, 0.005) (-5)	(-1.013, 0.0) (-6)	(-5.801, 0.001) (-7)	(-8.619, 0.0) (-9)
80	(-9.464, 0.022) (-3)	(-1.549, 0.0) (-4)	(-9.337, 0.004) (-5)	(-1.697, 0.0) (-6)	(-9.711, 0.001) (-7)	(-1.875, 0.0) (-8)
90	(-9.375, 0.017) (-3)	(-1.933, 0.0) (-4)	(-1.164, 0.0) (-4)	(-2.663, 0.0) (-6)	(-1.524, 0.0) (-6)	(-3.702, 0.0) (-8)
100	(-9.281, 0.013) (-3)	(-2.349, 0.0) (-4)	(-1.414, 0.0) (-4)	(-3.968, 0.0) (-6)	(-2.270, 0.0) (-6)	(-6.765, 0.0) (-8)
200	(-8.091, 0.003) (-3)	(-7.480, 0.0) (-4)	(-4.503, 0.0) (-4)	(-4.587, 0.0) (-5)	(-2.630, 0.0) (-5)	(-2.839, 0.0) (-6)
300	(-6.738, 0.001) (-3)	(-1.226, 0.0) (-3)	(-7.433, 0.0) (-4)	(-1.479, 0.0) (-4)	(-8.546, 0.0) (-5)	(-1.797, 0.0) (-5)
400	(-5.517, 0.001) (-3)	(-1.527, 0.0) (-3)	(-9.374, 0.0) (-4)	(-2.809, 0.0) (-4)	(-1.647, 0.0) (-4)	(-5.195, 0.0) (-5)
500	(-4.518, 0.000) (-3)	(-1.657, 0.0) (-3)	(-1.035, 0.0) (-3)	(-4.066, 0.0) (-4)	(-2.429, 0.0) (-4)	(-9.999, 0.0) (-5)
	(4, 1)	(4, 0)	(5, 1)	(5, 0)	(6, 1)	(6, 0)
100	(-3.761, 0.0) (-8)	(-1.162, 0.0) (-9)				
200	(-1.582, 0.0) (-6)	(-1.771, 0.0) (-7)	(-9.693, 0.0) (-8)	(-1.110, 0.0) (-8)		
300	(-1.010, 0.0) (-5)	(-2.200, 0.0) (-6)	(-1.215, 0.0) (-6)	(-2.708, 0.0) (-7)	(-1.477, 0.0) (-7)	(-3.345, 0.0) (-8)
400	(-2.967, 0.0) (-5)	(-9.674, 0.0) (-6)	(-5.432, 0.0) (-6)	(-1.811, 0.0) (-6)	(-1.005, 0.0) (-6)	(-3.403, 0.0) (-7)
500	(-5.829, 0.0) (-5)	(-2.474, 0.0) (-5)	(-1.420, 0.0) (-5)	(-6.154, 0.0) (-6)	(-3.491, 0.0) (-6)	(-1.536, 0.0) (-6)
	(7, 1)	(7, 0)	(8, 1)	(8, 0)		
400	(-1.871, 0.0) (-7)	(-6.410, 0.0) (-8)				
500	(-8.644, 0.0) (-7)	(-3.845, 0.0) (-7)	(-2.150, 0.0) (-7)	(-9.644, 0.0) (-8)		

TABLE III. Fourth-order multipole amplitudes $X_{J\lambda}^{(4)}(\omega)$ in atomic units. Numbers in parentheses represent powers of 10, which are adjusted to agree with those given in Table II. Column headings are in the format (J, λ) .

ω (Ry)	(1, 1)	(1, 0)	(2, 1)	(2, 0)	(3, 1)
5	-0.100 (-2)	0.0	-0.110 (-7)	0.133 (-11)	
10	-0.034 (-2)	0.0	-0.017 (-6)	0.018 (-10)	
20	-0.010 (-2)	0.0	-0.018 (-6)	0.002 (-9)	-0.003 (-9)
30	-0.042 (-3)	0.0	-0.002 (-5)	0.0	-0.001 (-8)
40	-0.023 (-3)	0.0	-0.002 (-5)	0.0	-0.001 (-8)
50	-0.014 (-3)	0.0	-0.001 (-5)	0.0	0.0
60	-0.010 (-3)	0.0	-0.001 (-5)	0.0	0.0
70	-0.007 (-3)	0.0	-0.001 (-5)	0.0	0.0
80	-0.005 (-3)	0.0	-0.001 (-5)	0.0	0.0
90	-0.004 (-3)	0.0	0.0	0.0	0.0
100	-0.003 (-3)	0.0	0.0	0.0	0.0
200	-0.001 (-3)	0.0	0.0	0.0	0.0

plitudes M_X and M_Y accurately to one part in 10^3 . In Table III the fourth-order correlation corrections $X_{J\lambda}^{(4)}(\omega)$ are listed with a similarly limited format.

Several comments are in order regarding Tables II and III. First, it should be noted that the imaginary parts of the amplitudes are rapidly decreasing functions of frequency compared with the real parts. As a consequence the entire amplitude is effectively dispersive (real) above 100 Ry. Second, it can be seen that for all frequencies considered the imaginary part of the magnetic-dipole amplitude vanishes; this fact can easily be understood in terms of the nonrelativistic behavior of Eqs. (3.7) for $\lambda=0$, $J=1$, discussed in Ref. 6(b). Third, the fourth-order amplitude, like the imaginary part of the second-order amplitude, is a rapidly decreasing function of frequency, indicating the appropriateness of treating Rayleigh scattering at high frequencies without concern for correlations.

In Table IV we list for each of the energies considered (a) the number of multipole amplitudes required in the calculation of the second-order cross section, (b) the fourth-order correlation correction, (c) the resulting theoretical Rayleigh-scattering cross section, and (d) the photoelectric cross section derived from the optical theorem using Eq. (5.3b).

In Fig. 4 we present angular distributions for several frequencies for Rayleigh scattering from He computed using the second-order amplitude, the second- plus fourth-order amplitude, and the "form-factor" approximation.⁹⁻¹² This latter approximation is simply the Thomson cross section modified to account for the momentum distribution of bound electrons. Specifically, we have

$$\frac{d\sigma}{d\Omega} \simeq \frac{1}{2} r_0^2 (1 + \cos^2 \theta) |F(q)|^2, \quad (5.4)$$

with

$$F(q) = 2 \int_0^\infty dr (G_1^2 + F_1^2) j_0(qr), \quad (5.5)$$

where $q = |\vec{k} - \vec{k}'|$. We see that the form-factor angular distribution is indistinguishable from that calculated from the second-order theoretical expressions for $\omega = 100$ and 500 Ry; furthermore, we see that the correlation contributes negligibly in this high-energy range. The remaining illustration in Fig. 3 for $\omega = 10$ Ry shows the importance of correlation, and the inadequacy of the form-factor approximation, at lower energies. The fact

TABLE IV. Theoretical second-order cross sections, fourth-order correlation corrections, and the resulting cross sections, including correlation, are tabulated together with σ_{pe} , the photoelectric cross section derived from the optical theorem. The column labeled J gives the number of multipoles used at each energy. Cross sections are given in b, and numbers in parentheses represent powers of 10.

ω (Ry)	J	σ_{2nd}	σ_{4th}	σ_{tot}	σ_{pe}
5	2	3.889	0.616	4.505	9.024 (5)
10	2	3.247	0.206	3.453	1.454 (5)
20	3	2.890	0.055	2.945	2.037 (4)
30	3	2.769	0.024	2.793	6.100 (3)
40	3	2.702	0.013	2.715	2.536 (3)
50	3	2.652	0.008	2.660	1.270 (3)
60	3	2.607	0.005	2.612	7.163 (2)
70	3	2.563	0.004	2.567	4.396 (2)
80	3	2.519	0.002	2.521	2.872 (2)
90	3	2.472	0.002	2.474	1.968 (2)
100	4	2.423	0.002	2.425	1.401 (2)
200	5	1.865	0.000	1.865	1.453 (1)
300	6	1.346	0.000	1.346	3.780
400	7	0.968	0.000	0.968	1.448
500	8	0.714	0.000	0.714	0.694

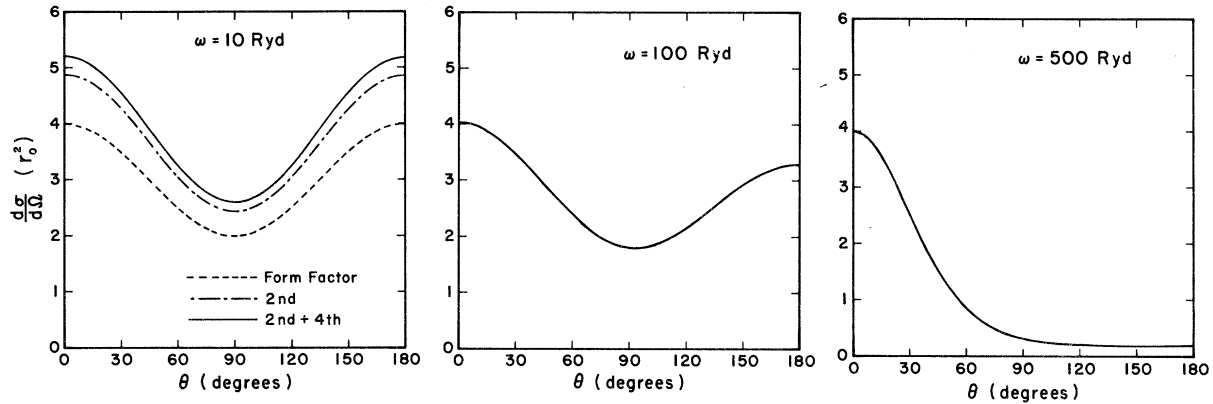


FIG. 4. Comparison of the second-order, fourth-order, and form-factor calculations of the Rayleigh-scattering differential cross section at different energies. For $\omega = 100$ and 500 Ry, the fourth-order correlation corrections are insignificant and the resulting differential cross section is indistinguishable from the form-factor approximation.

that the form-factor approximation is such a good approximation at high energies is due to the low Z of the atom under consideration (He; $Z = 2$). For higher- Z atoms, substantial modifications to the form-factor behavior are expected at high energies.¹³

In summary, the angular distribution of Rayleigh scattering for He varies smoothly between a dipole shape characterized by the electric polarizability at $\omega = 5$ Ry and a distribution given by the Thomson cross section modified by an atomic form factor above $\omega = 100$ Ry.

[†]Research supported in part by the National Science Foundation under Grant No. GP-42738.

*Work based on a dissertation to be submitted in partial fulfillment of the requirements for the Ph.D. degree by Chien-ping Lin at the University of Notre Dame.

¹G. E. Brown, R. E. Peierls, and J. B. Woodward, Proc. R. Soc. Lond. A **227**, 51 (1954); S. Brenner, G. E. Brown, and J. B. Woodward, *ibid.* A **227**, 59 (1954); G. E. Brown and D. F. Mayers, *ibid.* A **234**, 387 (1956); G. E. Brown and D. F. Mayers, *ibid.* A **242**, 89 (1957).

²G. W. F. Drake, Phys. Rev. A **9**, 2799 (1974); Dong-Liang Lin and G. Feinberg, *ibid.* **10**, 1425 (1974).

³We employ natural units $\hbar = c = 1$. The fine-structure constant $\alpha = e^2/4\pi = 1/137.03602$.

⁴The vector spherical harmonics \vec{Y}_{JLM} and $\vec{Y}_{JL}^{(\lambda)}$ are defined in A. I. Akhiezer and V. B. Berestetski, *Quantum Electrodynamics* (Interscience, New York, 1965). A discussion of Rayleigh scattering is found on pp. 484–491.

⁵The procedure used here is similar to that employed to analyze metastable decays in two-electron ions by

W. R. Johnson and Chien-ping Lin [Phys. Rev. A **9**, 1486 (1974)].

⁶Other applications of the auxiliary functions to Rayleigh scattering and related problems are found in (a) W. R. Johnson and F. D. Feiok, Phys. Rev. **168**, 22 (1968); (b) F. D. Feiok and W. R. Johnson, *ibid.* **187**, 39 (1969).

⁷V. G. Kaveeshwar, Kwong T. Chung, and R. P. Hurst, Phys. Rev. **172**, 35 (1968).

⁸A. Dalgarno and E. Kingston, Proc. R. Soc. Lond. A **259**, 424 (1960).

⁹W. Franz, Z. Phys. **95**, 652 (1935); **98**, 314 (1935).

¹⁰P. B. Moon, Proc. Phys. Soc. Lond. A **63**, 1189 (1950).

¹¹J. S. Levinger, Phys. Rev. **87**, 656 (1952).

¹²A. J. Nelm and I. Oppenheim, J. Res. Natl. Bur. Std. **55**, 53 (1955).

¹³V. Florescu and M. Gavrilă, in *Atomic Physics IV. Proceedings of the Fourth International Conference on Atomic Physics, Heidelberg, 1974*, edited by G. zu Putlitz, E. W. Weber, and A. Winnacker (Plenum, 1975).